Coupling metal concentrations and drift simulations for tracing emissions from offshore wind farms

Anna Ebeling [a,1] , Dominik Wippermann [a,b,1] , Tristan Zimmermann [a] , Ole Klein [a,c] , Torben Kirchgeorg [c] , Ingo Weinberg [c] , Anna Plass [c] , Simone Hasenbein [c] , Daniel Pröfrock [a,*]

[a] Helmholtz-Zentrum Hereon, Institute of Coastal Environmental Chemistry, Department Inorganic Environmental Chemistry, Max-Planck Str. 1, 21502 Geesthacht, Germany
[b] Universität Hamburg, Department of Chemistry, Inorganic and Applied Chemistry, Martin-Luther-King-Platz 6, 20146 Hamburg, Germany
[c] Federal Maritime and Hydrographic Agency (BSH), Wüstland 2, 22589 Hamburg, Germany

ARTICLE INFO

ABSTRACT

During the last decade offshore wind energy production has become an important source of renewable energy. To ensure safe operation during the lifetime of an offshore wind turbine, the steel structures need to be protected against corrosion. This work evaluates potential metal emissions and environmental impacts from galvanic anodes used for corrosion protection of offshore wind farms (OWFs) by applying a novel multi-tracer approach. A total of 235 surface water samples from different German North Sea OWFs were taken between 2016 and 2022 and analyzed for their concentration of 32 metals via online preconcentration/matrix removal ICP-MS/MS. The concentrations were assessed for temporal and spatial trends with an emphasis on the previously proposed OWF tracers Al, Cd, Pb, Zn, Ga and In. By comparing patterns of In concentrations and Gd anomalies together with modelled drift trajectories of water masses, a differentiation of riverine and OWF-induced metal load was achieved.

Results suggest that elevated In concentrations may be linked to OWF corrosion protection systems. Other metal concentrations remained within natural variability. This study demonstrates that the applied tracer approach is effective in identifying OWF-induced metal emissions. Furthermore, it highlights the necessity for long-term monitoring of these tracers to further investigate this emerging source of contamination.

1. Introduction

Offshore wind farms (OWFs) are pivotal for fulfilling the EU's goal to a sustainable energy transition and achieving climate neutrality by the year 2050 and the 2023's UN Climate Change Conference (COP28) agreement to triple renewable energy capacity by 2030. Nonetheless, OWFs introduce novel anthropogenic pressures to the marine environment. Effects include, but are not limited to, noise emissions, habitat changes or changes in ocean stratification (e.g. Christiansen et al. (2022); Degraer et al. (2021); Wright et al. (2020)). Another aspect is the emission of organic and inorganic substances from OWFs, that can occur during building and operation of the wind turbines and platforms, e.g.

through sediment remobilization, increased shipping for building and maintenance, scour protection and corrosion protection systems. Offshore structures are mainly made of steel and therefore require thorough corrosion protection against the harsh environmental conditions. Various corrosion protection systems are commonly applied, including impressed current cathodic protection (ICCP), corrosion allowance, organic coatings and galvanic anode cathodic protection. Galvanic anodes are consumed over time and could be a relevant source of metal emissions to the marine environment associated with OWFs (Kirchgeorg et al., 2018). For the protection of offshore wind structures in the German exclusive economic zone (EEZ) Al galvanic anodes made of an Al-Zn-In alloy are commonly used (Kirchgeorg et al., 2018). For a

lifespan of 27 years an average offshore wind monopile (6 m diameter, 26 m submerged in water and additionally coated) requires at least 2000 kg of Al galvanic anode material (VGB/BAW, 2018), resulting in a continuous emission of metals into the marine environment (Reese et al., 2020). This estimation has to be considered conservative, as the capacity of wind turbines and therefore the size of wind monopiles is increasing (Deutsche WindGuard GmbH, 2024; GWEC, 2024). In addition to the alloying metals Al, Zn (26,200 mg kg^{-1}–60,700 mg kg^{-1}) and In (143 mg kg^{-1}–231 mg kg^{-1}), Al anodes also contain a number of other metals, including, but not limited to, Ga (78.5 mg kg^{-1}–133 mg kg^{-1}), Pb (6.70 mg kg^{-1}–9.68 mg kg^{-1}) and Cd (0.255 mg kg^{-1}–6.920 mg kg^{-1}) (Reese et al., 2020).

While the analysis of sediment samples is commonly used to monitor long-term pollution and accumulation, the analysis of dissolved metal concentrations in seawater provides a current pollution status. The observation of short timescales is particularly interesting in the context of galvanic anodes, as they are in direct contact with the water and recent emissions could be detected. So far, only a few studies were dedicated to the investigation of emissions from galvanic anodes, mainly focusing on the bulk components Zn or Al (Degraer et al., 2019). Indeed, different studies observed measurable enrichments of anode-related metals in the aquatic environment. Bird et al. (1996) suggested that the measured increase of dissolved zinc in marinas and nearby estuary areas was caused by the use of Zn anodes for corrosion protection of yachts. Studies by Gabelle et al. (2012) regarding the usage of Al anodes within the port of Le Havre indicated that anodic dissolution did not increase the Al concentration in the harbor waters. However, a significant enrichment was observed in sediments sampled from undredged areas in the immediate vicinity (<20 m) of the Al anodes (Gabelle et al., 2012).

Overall, various studies highlighted the difficulties in assessing the impact of the galvanic anode dissolution on the concentrations of metals in the environment. This is especially true for metals with variable concentrations in the aquatic environment due to biogeochemical processes and/or anthropogenic sources (industry, shipping, etc.) like Al, Zn, Cd or Pb. Furthermore, potential source tracing is hindered by dilution effects in offshore environments. To trace potential metal emissions of galvanic anodes Reese et al. (2020) proposed to monitor the concentrations of In and Ga as tracers for offshore-wind-induced emissions. Within this context In and Ga are promising due to their comparably high mass fractions in Al anodes, low environmental background concentrations and the absence of other anthropogenic offshore sources. With OWFs located mostly in shallow waters and relatively close to the coast, rivers and coasts are also a source of metal input into seawater. A tool for source tracing of riverine inputs into the North Sea is the Gd anomaly (Hatje et al., 2016; Kulaksız and Bau, 2007; Siems et al., 2024). The rare-earth element (REE) Gd is broadly used in magnetic resonance imaging (MRI) contrast agents. The Gd complexes are very water soluble and long-term stable in natural waters. They are not efficiently removed by wastewater treatment plants and are discharged via rivers into coastal waters, resulting in a positive Gd anomaly (Kulaksız and Bau, 2007). Furthermore, backward drift simulations of the surface water can support the interpretation of measurement data, as they give valuable information about the short-term trajectory (several days) of the sampled water masses. For the German North Sea drift simulations are available based on work by Callies (2021); Callies et al. (2017).

With the lack of metal data in the vicinity of OWFs (Schulz-Stellenfleth et al., 2023) a sound assessment of the impact of OWFs on the marine environment is currently not possible. The limited number of studies on metal emissions associated with galvanic anodes from OWFs into surrounding sediments indicate possible OWF-induced sediment contamination (Degraer et al., 2019; Ebeling et al., 2023d; Wang et al., 2023). However, currently available studies also emphasize the need for further investigations to assign the observed results to emissions caused by OWFs with higher confidence.

This study provides concentrations of 32 metals for water samples from OWFs in the German Bight sampled over a period of six years. To our knowledge this is the first large scale dataset presenting dissolved metal data from the vicinity of OWFs. Our study focusses on the proposed tracer elements for corrosion protection of OWFs (Al, Cd, Ga, In, Pb and Zn), which are discussed in detail regarding their temporal variation in the German North Sea. Furthermore, the study presents a new approach for source assignment of inorganic emissions from OWFs, whereby Gd anomalies are calculated and compared to In concentrations and water mass back trajectories. The approach developed offers a new possibility for environmental monitoring and source allocation of emissions from corrosion protection.

2. Materials and methods

The overall methodological approach of this study is structured in three parts: Sampling (chapter 2.2) and sample preparation (chapter 2.3), analytical determination of analytes in the samples (chapters 2.4, 2.5.1 and 2.5.2) and assessment of the collected data (see Fig. 1A). Tools and methods enabling the assessment are described in the chapters 2.5.3 to 2.5.6.

2.1. Reagents and materials

All preparatory laboratory work was performed in a class 10,000 or class 1000 clean room inside a class 100 clean bench. Type I reagent-grade water (18.2 MΩ cm) was obtained from a Milli-Q Integral water purification system equipped with a Qpod-Element polishing system (Merck-Millipore, Darmstadt, Germany).

Analytical grade HNO$_3$ (w = 65 %, Fisher Scientific GmbH) and analytical grade HCl (w = 30 %, Carl Roth GmbH + Co. KG, Karlsruhe, Germany) were further purified by double sub-boiling either in perfluoralkoxy-polymer (PFA)-subboling stills (DST-4000 & DST-1000, Savillex, Minnesota, USA) or in a cascade of two quartz stills (AHF Analysentechnik, Tübingen, Germany). The purified acids were stored in acid cleaned PFA bottles. Optima grade glacial acetic acid and optima grade ammonia solution (w = 20–22 %) (Fisher Scientific, Schwerte, Germany) were used without further purification to produce 4 mol L^{-1} ammonium acetate buffer adjusted to pH 6.0 ± 0.2. The reference waters CASS-6 and NASS-7 (National Research Council Canada) were routinely measured for method validation. External calibration standard solutions for quantification (all traceable to NIST standards) were prepared from custom-made multi-element standards of different composition (Inorganic Ventures, Christiansburg, USA). Single-element ICP standards (1 g L^{-1}) of Al, In, Nb, Tl, Ti, W were obtained from Merck Millipore.

All plastic (LDPE and PP) consumables were pre-cleaned by established protocols in solutions of HNO$_3$ (w = 1–2 %) for a minimum of one week. Before usage the material was rinsed with MilliQ water and dried inside a class 100 clean bench inside a clean room.

2.2. Sampling

A total of 235 water samples of the German North Sea were obtained during six ship sampling campaigns with the research vessels Atair (Federal Maritime and Hydrographic Agency, BSH) in 2018 (AT261), 2019 (AT275), 2021 (AT004), 2022 (AT010), and the Ludwig Prandtl (Hereon) in 2016 (LP20160725) and 2020 (LP20200629). Due to logistical challenges and weather conditions not all sampling stations were sampled every year. At each station water samples were taken at a depth of 10 m using a metal-free, pre-cleaned 10 L GO FLO water sampler (General Oceanics, Miami, USA). Samples cover different OWF areas within the German EEZ (see Fig. 1), which utilize different setups for corrosion protection. Table 1 gives an overview of the number of samples taken in the respective OWF areas per year. A list of all samples including the geographical coordinates can be found in electronic supplemental material (ESM) Table A1.
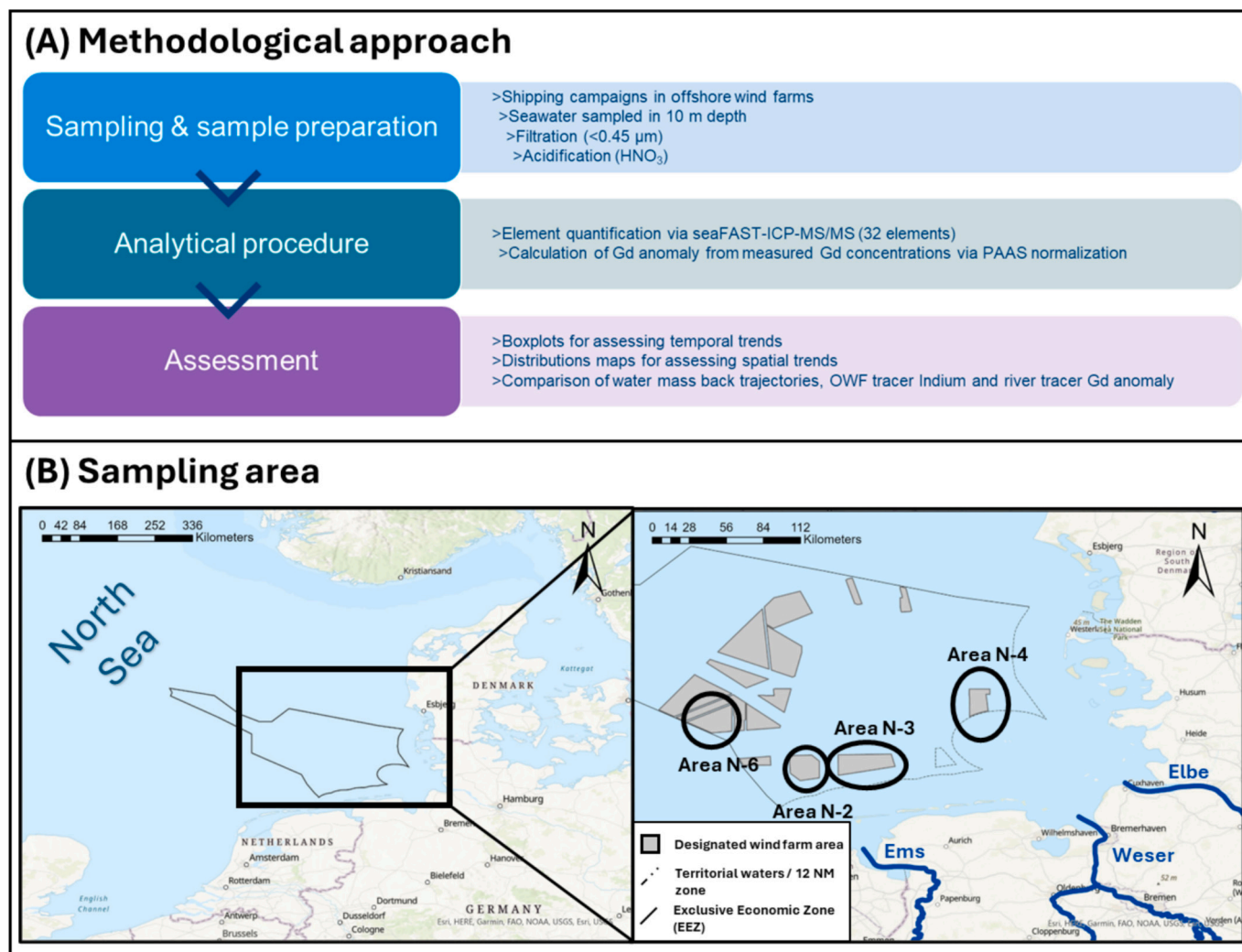
Fig. 1. A: Flow chart of the methodological approach. B: Sampling areas in and around OWFs in the German Bight (grey areas) within the German exclusive economic zone (dashed line). The investigated areas are labeled according to the site development plan for the German North Sea and Baltic Sea (BSH, 2023a, 2023b).

Table 1
Numbers of sampled stations per campaign and area.

	Area N-2	Area N-3	Area N-4	Area N-6
LP20160725 (2016)	2	1	18	–
AT261 (2018)	12	23	19	–
AT275 (2019)	13	23	36	11
LP2020629 (2020)	–	11	26	–
AT004 (2021)	2	3	10	7
AT010 (2022)	3	3	11	1

2.3. Sample preparation

The water samples were pressure filtrated directly on board inside a class 100 clean bench (LP20160725, AT261 and AT275) or shortly after the sampling in the home laboratory in a clean room (LP20200629, AT004, AT010) using pre-cleaned PFA pressure filtration units (AHF Analysentechnik, Germany) and acid leached 0.4 μm Whatman Nucleopore track etched polycarbonate membranes (Whatman, Dassel, Germany) (Przibilla et al., 2023). After filtration the samples were acidified with HNO_3 and stored in acid cleaned LDPE bottles. The filtered samples were doubly packed in LDPE bags and stored at 4 °C in the dark until measurement.

2.4. Instrumentation

2.4.1. Online matrix removal and preconcentration

A seaFAST SP2 (Elemental Scientific, Omaha, USA), equipped with two columns filled with Nobias chelate-PA1 (HITACHI High-Tech Fielding Corporation, Tokyo, Japan) resin, was used for matrix removal and preconcentration of the analytes. The seaFAST system was operated according to supplier recommendations with a 4 mol L^{-1} ammonia acetate buffer (pH = 6.0 ± 0.2) and 1.5 mol L^{-1} HNO_3 as eluent. An external calibration, stabilized in diluted HNO_3 with w = 0.14 %, ranging from 0.1 ng L^{-1} to 100 ng L^{-1} for In, 10 ng L^{-1} to 10,000 ng L^{-1} for Al and 1 ng L^{-1} to 1000 ng L^{-1} for all other analytes (Ti, V, Mn, Fe, Co, Ni, Cu, Zn, Ga, Y, Mo, Cd, Sn, REE, W, Pb and U) was applied using traceable custom-made multi-element standards. The automated dilution function of the seaFAST based on two stock solutions (20 ng L^{-1} and 1000 ng L^{-1}) was used for calibration. A 1 μg L^{-1} Nb internal standard solution was dosed online to every sample allowing for drift correction if necessary. Details on the method performance can be found elsewhere (Ebeling et al., 2022).

2.4.2. ICP-MS/MS

The seaFAST system was coupled online to an ICP-MS/MS system (Agilent 8900, Agilent Technologies, Tokyo, Japan). The instrument was

optimized before every measuring batch using a tuning solution containing Li, Co, Y, Ce and Tl. For samples of the first four campaigns (LP20160725, AT261, AT275, LP20200629) the ICP-MS/MS instrument was operated in O_2 mode for the quantification of Ti, Y and REE and in He mode for the quantification of Al, V, Mn, Fe, Co, Ni, Cu, Zn, Ga, Mo, Cd, In, Sn, W, Pb and U (Ebeling et al., 2022). The samples of the campaigns AT004 and AT010 were measured in a combined method for all analytes with the ICP-MS/MS instrument operating in He/H_2 (mixture) mode (Przibilla et al., 2023). The ICP-MS/MS was equipped with x-lenses for measurements in O_2 mode and with either x- or s-lenses in He mode. Measurements in He/H_2 mode were solely conducted using s-lenses to maximize sensitivity. Setting details and typical tuning conditions of the ICP-MS/MS can be found in ESM Table A2. A list of all measured isotopes, mass-shifts and gas modes used for quantification in this study can be found in ESM Table A3. Procedural limits of detection (*LOD*) and limits of quantification (*LOQ*) for the six sampling campaigns can be found in ESM Table A4. Detailed validation parameters of various reference materials can be found elsewhere (Ebeling et al., 2022).

2.5. Data evaluation and presentation

2.5.1. Multi-element analysis

Multi-element data were processed using MassHunter version 4.4 or higher (Agilent Technologies, Tokyo, Japan) in time-resolved mode and a custom written Excel spreadsheet.

The isobaric interference of ^{115}Sn on ^{115}In was corrected for by peak stripping as implemented in MassHunter using the signal of ^{118}Sn and the isotopic abundances (de Laeter et al., 2003).

Procedural *LODs* and *LOQs* were calculated in accordance with the blank value method described in DIN 32645:2008-11 (DIN e.V. (ed.), 2008) from procedural filtration blanks ($n > 3$ per campaign).

The significant number of digits of concentrations are given according to GUM and EURACHEM guidelines, whereby the uncertainty determines the significant number of digits to be presented with the value (Eurachem/Citac, 2012).

2.5.2. Calculation of normalized REE patterns and Gd anomaly

As a proxy to calculate possible anthropogenic influences, the REE concentrations were normalized using the Post-Archean Australian Average Shale (PAAS) (McLennan, 1989). Gd anomalies Gd/Gd* were quantified using Eq. (1) (Kulaksız and Bau, 2007) with the Index SN indicating shale normalized REE values and Gd* being the extrapolated undisturbed Gd concentration.

$$\frac{Gd_{SN}}{Gd_{SN}^*} = \frac{Gd_{SN}}{10^{2\log Sm - \log Nd}} \qquad (1)$$

2.5.3. Data assessment criteria

The measured concentrations of Cd, Pb and Zn are compared to the Background Reference Concentrations (BRC) of the Northern North Sea as provided by OSPAR (OSPAR, 2005), the Acceptable Annual Average Concentration Environmental Quality Standard (AA-EQS) according to the Water Framework Directive (WFD) (EU, 2008) and to the average concentration in 10 m water depth in the German North Sea (BSH North Sea) monitored by the BSH (BSH, 2016).

To the best of our knowledge, monitoring data do not exist for the tracer metals Al, Ga and In. Thus, the measured concentrations are compared to concentration ranges of North Atlantic surface ocean water (Kremling et al., 1999) and to concentrations measured by Ebeling et al. (2022) in the seawater reference material ERM CA-403 (Joint Research Centre, Geel, Belgium), which was taken in the North Sea outside of the Belgian coast (Southern Bight) in 2010. The comparison base values are listed in Table 2.

2.5.4. Data presentation

The measured concentration data is presented in box plots,

indicating the median of the respective data volume (line, P50) with 98 % confidence interval, the interquartile range (P25 – P75) limited by the lower and upper limit of the box and the extreme values of the respective data series. Measured values with a distance of 1.5 interquartile ranges that exceed the interquartile limits are identified by dots as outliers. Numbers in the box plots indicate minimum and maximum values excluding outliers.

2.5.5. Water masses drift trajectories

Drift trajectories were calculated with the PELETS-2D program (Callies et al., 2011) through the DriftApp Tool[2] for surface layer currents. Based on the coordinates and sampling time the model allows to calculate the trajectories for a period of five days prior to the time of sampling.

2.5.6. Distribution maps

Distribution maps showing selected parameters were created using ArcGIS® Pro by Esri®; basemap by ArcGIS (2023), additional layers from BSH (2023a). ArcGIS® and ArcMap™ are the intellectual property of Esri and are used herein under license.

3. Results

In total concentrations of 32 metals were measured in 235 North Sea water samples. The complete data set for all measured metals can be found in ESM Table A1 and in the data repository PANGAEA (Ebeling et al., 2023a; Ebeling et al., 2023b; Ebeling et al., 2023c; Klein et al., 2022; Wippermann et al., 2025a; Wippermann et al., 2025b). The following section describes the distribution of selected metals (Al, Cd, Ga, In, Pb, Zn) in samples obtained during the six sampling campaigns. The selection of the presented metals is based on the suggested tracer metals by Reese et al. (2020) as proxy for potential emissions originating from galvanic anodes applied for corrosion protection in OWFs.

3.1. Metal concentrations

3.1.1. Cadmium

Cd shows concentrations between 9.49 ng L^{-1} ± 0.04 ng L^{-1} and 40.7 ng L^{-1} ± 0.4 ng L^{-1}, (see Fig. 2A, the distribution map in ESM Fig. A1 and a high-resolution box plot in ESM Fig. A2). Overall, inter-year variability of the Cd concentrations for most areas is within the OSPAR BRC range (8 ng L^{-1}–25 ng L^{-1}) with notable differences between each year. Cd concentrations exceeding the OSPAR BRC are found within Area N-3 (22.2 ng L^{-1} ± 1.3 ng L^{-1}–29.0 ng L^{-1} ± 0.5 ng L^{-1} for 2019 and 16.574 ng L^{-1} ± 0.001 ng L^{-1} - 35 ng L^{-1} ± 26 ng L^{-1} for 2021), as well as for Area N-4 (26.6 ng L^{-1} ± 0.2 ng L^{-1}–40.7 ng L^{-1} ± 0.4 ng L^{-1} for 2019). The BSH Cd concentration range of 12 ng L^{-1}–52 ng L^{-1} (N. Sea) exceeds the upper range of the OSPAR BRC. Samples from 2019 (03/19) featured the highest Cd concentrations for all investigated areas.

3.1.2. Lead

Pb concentrations range between 1.45 ng L^{-1} ± 0.08 ng L^{-1} and 39 ng L^{-1} ± 27 ng L^{-1}, as shown in Fig. 2B. Furthermore, a distribution map of the Pb concentrations can be found in ESM Fig. A3 and a high-resolution boxplot in ESM Fig. A4. Between 2016 and 2020 the concentrations of Pb range mostly below the OSPAR BRC (10 ng L^{-1}–20 ng L^{-1}) and the monitoring values of the BSH (10 ng L^{-1}–520 ng L^{-1}) (N. Sea), except for the samples from Area N-6, with values (14.6 ng L^{-1}–18.1 ng L^{-1}) within the OSPAR BRC. In 2021 and 2022 generally higher concentrations were determined. While in Area N-2 the OSPAR BRC is not exceeded, in Areas N-3, N-4 and N-6 Pb concentrations of >23.5 ng L^{-1} were measured in 2021 and for Area N-3 also in 2022.

---

[2] https://hcdc.hereon.de/drift-now/.

Table 2

Criteria for evaluating the dissolved metal content in marine waters.

	$c(Cd)$ / ng L^{-1}	$c(Pb)$ / ng L^{-1}	$c(Zn)$ / ng L^{-1}	$c(Al)$ / ng L^{-1}	$c(Ga)$ / ng L^{-1}	$c(In)$ / ng L^{-1}
BRC (OSPAR)[a]	8–25	10–20	250–450			
AA-EQS (WFD)[b]	200	7200				
BSH North Sea[c]	12–52	10–520	63–3800			
North Atlantic Surface Ocean Water[d]				810–1160	1.7–2.1	0.3
Southern Bight (North Sea)[e]				2500 ± 1000	6.3 ± 1.6	0.057 ± 0.010

[a] BRC: Background Reference Concentrations of the Northern North Sea. OSPAR (OSPAR, 2005).
[b] AA-EQS: Annual Average Concentration Environmental Quality Standard (EU, 2008).
[c] BSH North Sea (N. Sea): Monitored metal concentration in German Bight's coastal waters (10 m sampling depth) between 2010 and 2014, monitored by the BSH, accessed through the database MUDAB (UBA, 2024).
[d] North Atlantic surface Ocean water (Kremling et al., 1999).
[e] Southern Bight: Values of reference material ERM CA-403 (Ebeling et al., 2022).

3.1.3. Zinc

Zn features concentrations between 247 ng L^{-1} ± 2 ng L^{-1} and 2180 ng L^{-1} ± 20 ng L^{-1}, as shown in Fig. 2C. Furthermore, a map of the Zn concentrations of all analyzed samples can be found in ESM Fig. A5 and a high-resolution boxplot in ESM Fig. A6. Overall, the Zn concentrations span between the OSPAR BRC (250 ng L^{-1}–450 ng L^{-1}) and the monitoring values of the BSH (63 ng L^{-1}–3800 ng L^{-1}) (N. Sea). Samples with higher concentrations than the OSPAR BRC are located in Area N-3 in 2021 and Area N-4 in 2018 and 2019, with notable intra-area variability and minimum values still within the range of BSH monitoring values.

3.1.4. Aluminum

Al shows concentrations between 78 ng L^{-1} ± 5 ng L^{-1} and 670 ng L^{-1} ± 40 ng L^{-1} (see Fig. 3A, the distribution map in ESM Fig. A7 and a high-resolution boxplot in ESM Fig. A8). All analyzed Al concentrations are about one order of magnitude lower than concentrations in the reference material ERM CA-403 (seawater collected from the Southern Bight outside the coast of Belgium (North Sea)) (Ebeling et al., 2022). Kremling et al. (1999) published Al concentrations for North Atlantic surface ocean water ranging between 810 ng L^{-1} and 1160 ng L^{-1}, which are in the same order of magnitude as the Al concentrations presented in this study. The Al concentrations are predominantly evenly distributed within the investigated areas. Area N-4 and Area N-6 show occasionally higher Al concentrations (>400 ng L^{-1}), but median concentrations are within the range of Area N-2 and Area N-3. Area N-6 (03/19) shows the highest Al concentrations (480 ng L^{-1} ± 10 ng L^{-1}–670 ng L^{-1} ± 40 ng L^{-1}) leading to the only median concentration above 400 ng L^{-1} of Al in this study.

3.1.5. Gallium

Ga features concentrations between 1.37 ng L^{-1} ± 0.05 ng L^{-1} and 4.9 ng L^{-1} ± 0.5 ng L^{-1} (see Fig. 3B, the distribution map in ESM Fig. A9 and a high-resolution boxplot in ESM Fig. A10). The highest Ga concentrations were found in Area N-4 in 2019 and 2022. Concentrations vary between the sampling years, except for one sample from Area N-4 in 2019 with $c(Ga)$ = 4.9 ng L^{-1} ± 0.5 ng L^{-1}, all measured Ga concentrations are below the concentration range of 4.7 ng L^{-1}–7.9 ng L^{-1} reported for the reference material ERM CA-403 (Ebeling et al., 2022). Published Ga concentrations of North Atlantic surface ocean water range from 1.7 ng L^{-1} to 2.1 ng L^{-1} (Kremling et al., 1999). Even though the data of this study features slightly higher concentrations of some samples, Ga concentrations are within the same order of magnitude. For Area N-2 (07/16) and (03/19), as well as for Area N-4 (07/16) concentrations are in good agreement with Kremling et al. (1999). Overall, Ga concentrations in this study were within a narrow range.

3.1.6. Indium

The In concentrations range between 0.011 ng L^{-1} ± 0.001 ng L^{-1} and 0.27 ng L^{-1} ± 0.15 ng L^{-1} (see Fig. 3C, the distribution map in ESM Fig. A10 and a high-resolution boxplot in ESM Fig. A11). The highest In concentrations were found in Area N-4 (06/20), (04/21) and (04/22), as well as for two sampling locations in Area N-3 in (04/21). Yet, all area-specific median In concentrations in this study are below the published concentration for North Atlantic surface ocean water of 0.3 ng L^{-1} (Kremling et al., 1999). Ebeling et al. (2022) reported significantly lower In concentrations (0.057 ng L^{-1} ± 0.010 ng L^{-1}) for the Southern Bight seawater ERM CA-403, which is in good agreement with In concentrations presented in this study. Median In concentrations are within or slightly below the range of In for the Southern Bight except for Area N-2 (04/21), Area N-3 (04/21), Area N-4 (06/20) and (04/21) and Area N-6 (04/21), which show higher In median concentrations. The highest variability of In concentration was observed in Area N-3 (04/21) (0.075 ng L^{-1} ± 0.008 ng L^{-1}–0.26 ng L^{-1} ± 0.12 ng L^{-1}) and Area N-4 (06/20) (0.029 ng L^{-1} ± 0.008 ng L^{-1}–0.269 ng L^{-1} ± 0.028 ng L^{-1}) and (04/22) (0.024 ng L^{-1} ± 0.005 ng L^{-1} – 0.27 ng L^{-1} ± 0.15 ng L^{-1}). Overall, In concentrations showed the most heterogenous distribution compared to Al and Ga.

3.2. Gadolinium anomaly

The Gd anomaly ranges between 1.00 ± 0.09 and 4.00 ± 0.64 as shown in Fig. 4, while the Gd concentration ranges between 0.78 ng L^{-1} ± 0.21 ng L^{-1} and 6.4 ng L^{-1} ± 0.9 ng L^{-1} (see ESM Table 1). A map of the Gd anomaly for all campaigns can be found in ESM Fig. A13 and a high-resolution boxplot in ESM Fig. A14.

All analyzed samples showed positive anomalies (>1.0) and most samples even exceeded the threshold value of 1.2 indicating an anthropogenically induced Gd anomaly. Highest Gd anomalies were observed for Area N-4 in 2021 (1.7 ± 2.1–4.0 ± 0.64) and Area N-2 in 2016 (2.9 ± 0.4–3.15 ± 0.11). Overall, the lowest Gd anomalies were observed in 2022 in all areas (1.00 ± 0.09–1.7 ± 0.42). While Siems et al. (2024) reported similar Gd concentrations for seawater from the German Bight in 2021 (0.69 ng L^{-1} ± 0.05 ng L^{-1} to 6.0 ng L^{-1} ± 2.3 ng L^{-1}) the respective Gd anomalies span a wider range (1.31 ± 0.22 and 8.17 ± 2.42) than the anomalies found in the OWF samples of this study (see Fig. 4).

4. Discussion

4.1. Variability of metal concentrations

Cd and Zn are so-called recycled or nutrient type metals, which are involved in biological activity and are characterized by long residence times in seawater (10^3–10^5 years) (Bruland, 1980; Kremling et al., 1999). Therefore, possible anthropogenic emissions from e.g. galvanic anodes tend to stay within the water bodies for a longer time compared to other metals. Data from this study does not indicate an accumulation of Cd within the water in and near OWFs during the period studied, even though temporarily increased concentrations were found (see Fig. 2A). A sound emission allocation is currently difficult due to the low mass fractions of Cd in the Al anodes (Reese et al., 2020), the already known elevated Cd concentrations compared to BRC in the German Bight and
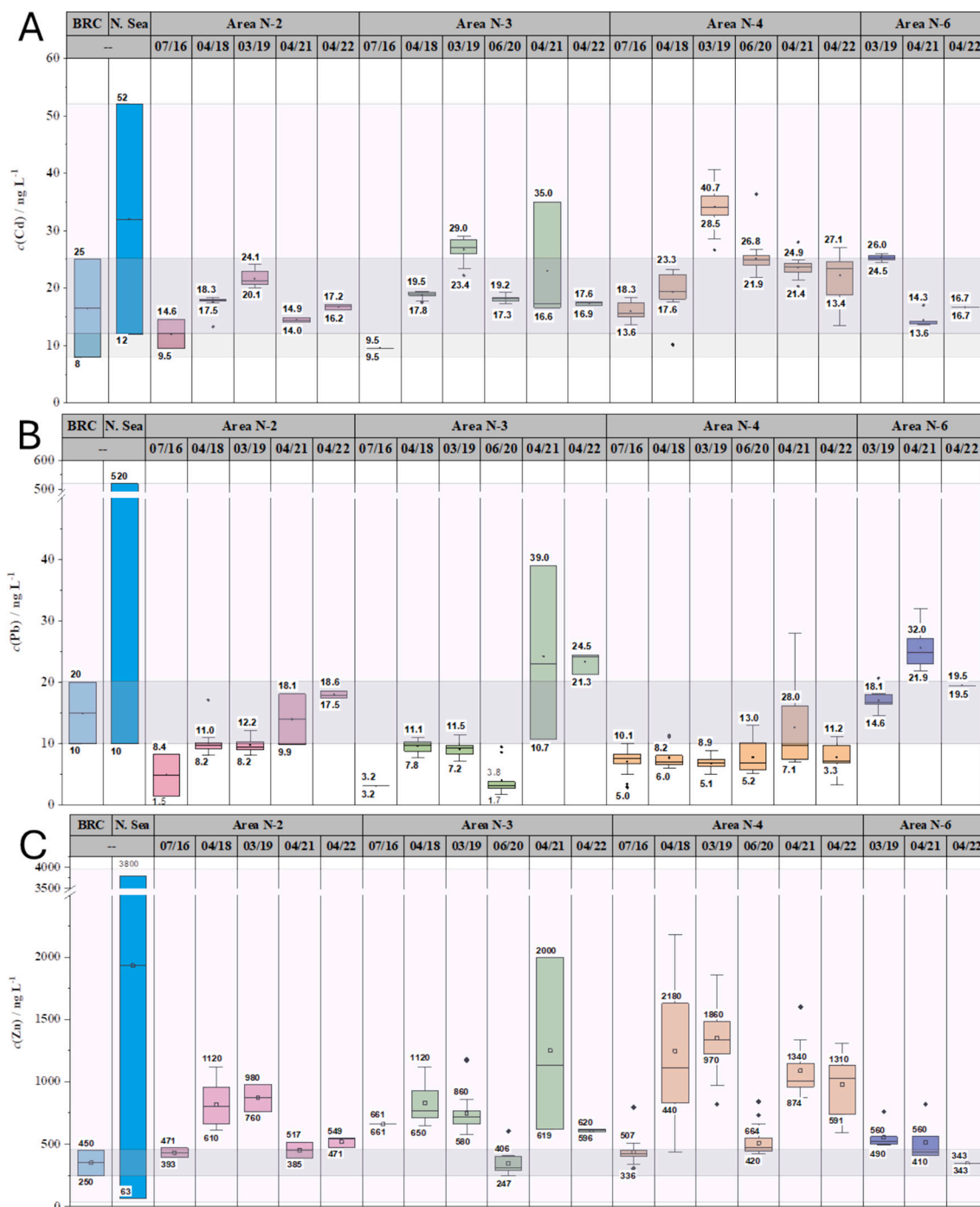
Fig. 2. Metal concentrations in North Sea waters in and around OWFs of the German Bight for the monitoring metals (A) Cd, (B) Pb and (C) Zn. The samples are grouped according to the designated areas (see Fig. 1). Reference values are given as BRC = Background Reference Concentrations of the Northern North Sea as provided by OSPAR (OSPAR, 2009a); N. Sea. = BSH North Sea: Known concentration in 10 m depth in coastal waters of the German Bight monitored by the BSH between 2010 and 2014 and accessed through the MUDAB database (UBA, 2024).

other anthropogenic Cd sources.

Like Cd, temporarily elevated Zn concentrations were found throughout different years. Especially Area N-4 showed a high variability and in four of the six investigated years Zn concentrations exceed BRC. Due to the residence time of Zn in seawater, concentration changes caused by galvanic anodes are expected to be measurable first within the water body, especially with Zn being the second most abundant metal in Al anodes (Reese et al., 2020). Indeed, current data does not indicate an increasing trend for Zn concentrations within the investigated period from OWFs. Because of various other anthropogenic Zn emissions, such

as inputs via rivers (Zimmermann et al., 2020) or galvanic Zn anodes used for ships (OSPAR, 2009b), it is difficult to precisely allocate the emission source. However, based on their toxicological relevance and potential as tracer for possible emissions from corrosion protection of OWFs, Cd and Zn should be routinely measured in the water matrix as part of future monitoring.

Pb is a scavenged metal, which means its concentration in seawater decreases with increasing depth due to its affinity to bind to particles (Kremling et al., 1999). Indeed, the residence time of Pb is hardly assessable due to ocean currents and anthropogenic influences (e.g.
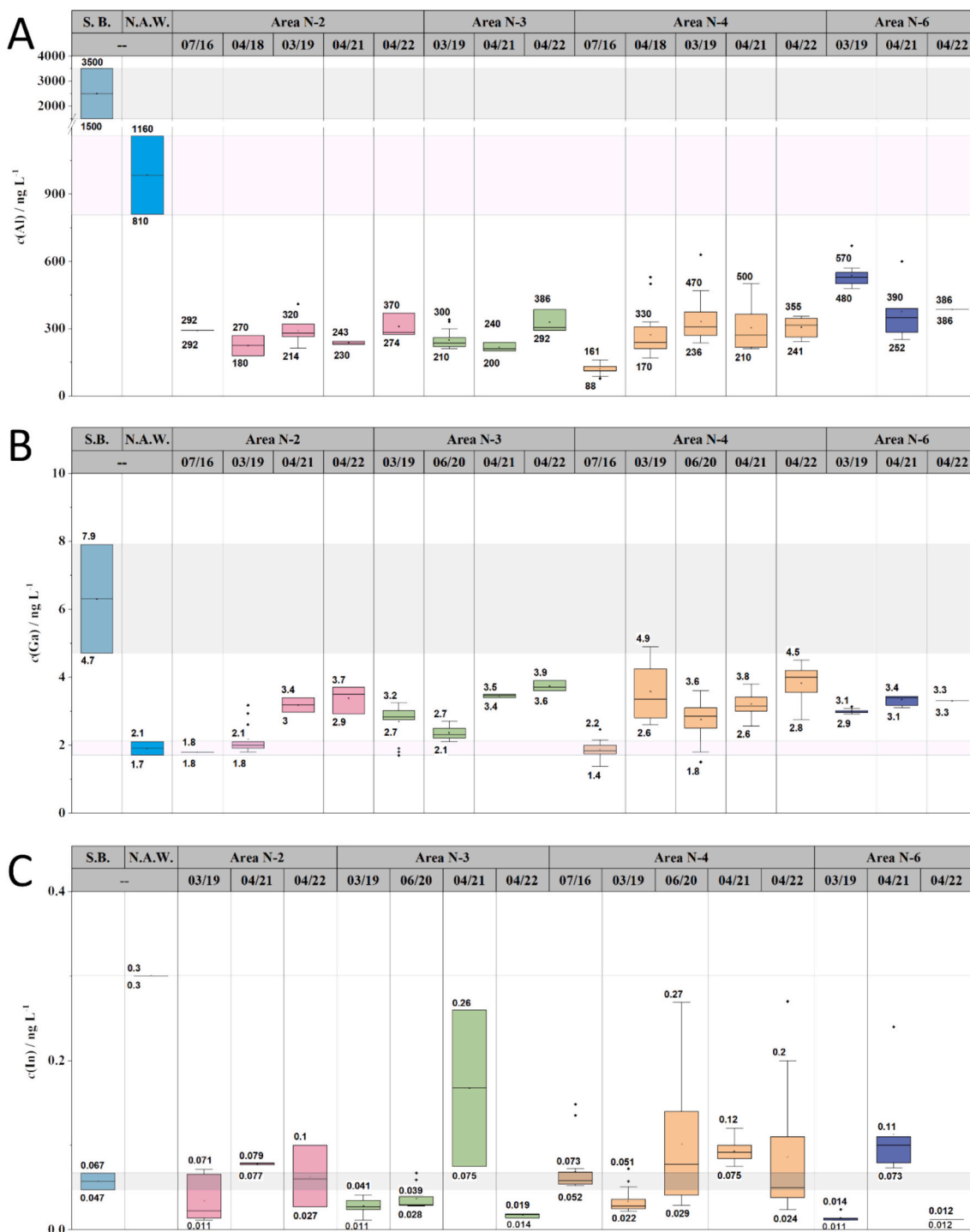
Fig. 3. Metal concentrations of the selected tracer metals in North Sea waters in and around OWFs of the German Bight for (A) Al, (B) Ga and (C) In. The samples are grouped according to the designated areas (see Fig. 1). Reference values are given as S.B. = Southern Bight: Values of reference material ERM CA-403 (Ebeling et al., 2022) and N.A.W = North Atlantic surface Ocean water (Kremling et al., 1999).

shipping). Data from this study showed the highest variability of Pb concentrations in 2021 (see Fig. 2B). However, as a particle-active metal with comparably low residence time at the water surface (approximately 1 year) (Nozaki et al., 1976), elevated Pb concentrations would subsequently lead to elevated Pb mass fractions in the surrounding sediments. Yet, in a previous study, no accumulation of Pb in sediment samples near OWFs of the German North Sea were measurable neither in 2021 nor 2022 (Ebeling et al., 2023d). The elevated Pb concentrations in 2021 might also relate to other sources than the OWFs as anthropogenic

Pb is introduced into the marine environment through a wide variety of sources, such as industrial applications directly in the marine environment but also from riverine inputs transporting anthropogenic inputs or through combustion processes of fossil fuels (Komárek et al., 2008). Due to its diverse sources in the marine environment, the complex transport processes within the German Bight and its short residence time in seawater, it is currently not possible to directly relate partly elevated Pb concentrations in the vicinity of OWFs to corrosion protection-related releases.
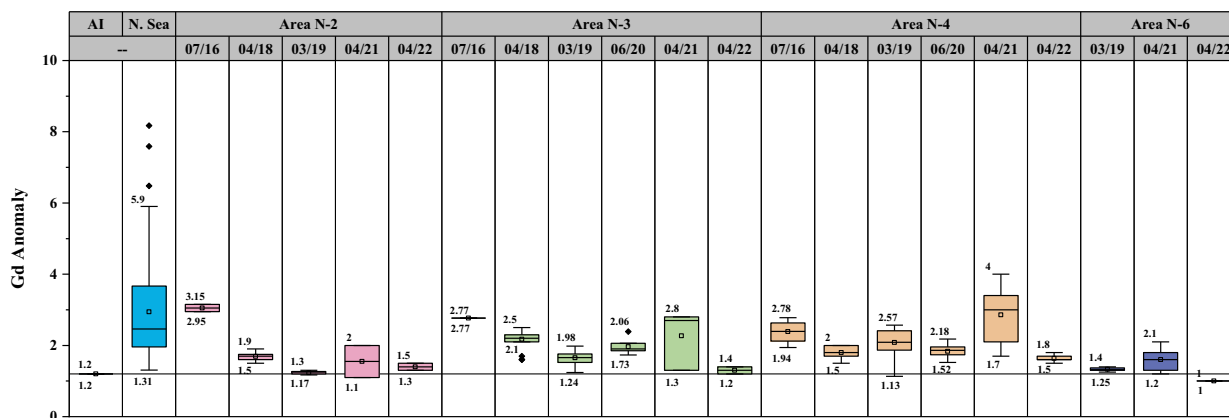
AI	N. Sea	Area N-2					Area N-3						Area N-4						Area N-6		
--	--	07/16	04/18	03/19	04/21	04/22	07/16	04/18	03/19	06/20	04/21	04/22	07/16	04/18	03/19	06/20	04/21	04/22	03/19	04/21	04/22

Fig. 4. Gadolinium anomaly in North Sea waters in and around OWFs of the German Bight. The samples are grouped according to the designated areas (see Fig. 1). Reference values are given as AI = Threshold for anthropogenic influence (Bau and Dulski, 1996); N.Sea = North Atlantic surface Ocean water (Siems et al., 2024).

As the major component of galvanic Al anodes, the released Al amount will be significantly higher than all other metals. Al concentrations in this study ranged between 78 ng $L^{-1} \pm 5$ ng L^{-1} and 670 ng $L^{-1} \pm 40$ ng L^{-1} with only minor differences between sampling locations and years. Currently there are no official threshold values for Al in North Sea waters and Al is not monitored on a regular basis (BSH, 2016). In contrast, Australian guidelines suggest a low reliability marine trigger value for Al of 500 ng L^{-1} (ANZECC and ARMCANZ, 2000) which some of the samples, as well as reference values of this study, exceed (see Table 2). Golding et al. (2015) proposed to increase this value to 24 µg L^{-1} for 95 % species protection based on their studies of Al exposure to different water organisms. This proposed threshold is one order of magnitude higher than data presented in this study and suggests that current Al concentrations in and around OWFs of the German North Sea do not represent a risk to marine organisms. However, it has to be considered that Al is a particle active metal with a relatively short residence time of 4 weeks to 4 years at surface levels and 50–150 years in the deep sea (Orians and Bruland, 1986). In addition, the low solubility in seawater leads to the expectation that increased dissolved Al concentrations will only be measurable very close to the emission source, i. e. the galvanic anode, and that in the long term Al from the anodes will tend to accumulate in the sediment. In fact, neither this study nor a recent study by Ebeling et al. (2023d) report increased Al levels in marine sediment or water near OWFs in the German North Sea in the period of 2016–2022. Furthermore, Al is the second most abundant metal in the upper continental crust (Rudnick and Gao, 2003) and is introduced into the marine environment by rivers with high Al concentrations. Prange et al. (2001) reported 2 µg L^{-1} to 200 µg L^{-1} within the River Elbe, which is one to three orders of magnitude higher than Al concentrations measured in this study. Currently results do not indicate measurable Al inputs in the marine environment caused by OWFs.

To the best of our knowledge no Ga concentrations of North Sea water have been published up to now. Wuttig et al. (2019) reported Ga concentrations of open ocean water (southern Indian Ocean) derived from the GEOTRACES program of around 0.56 ng L^{-1} to 0.98 ng L^{-1}. Furthermore, Ebeling et al. (2022) published consensus values e.g. for the ocean water reference materials CASS-4 (3.1 ng $L^{-1} \pm 1.7$ ng L^{-1}) and NASS-6 (1.9 ng $L^{-1} \pm 1.9$ ng L^{-1}), as well as ERM CA-403 (6.3 ng $L^{-1} \pm 1.6$ ng L^{-1}; Southern Bight water). Looking at the most recent sampling times (2020–2022), Area N-2, Area N-3 and Area N-4 show minor increasing trends (see Fig. 3B), but are still lower than the Southern Bight water ERM CA-403 (Ebeling et al., 2022). The biogeochemistry of Ga remains largely unexplored. Overall, Ga is expected to have similar geochemical properties to Al and is sometimes used as a geochemical tracer analog with Al (Yuan et al., 2021). Due to its interactions with suspended solids and the associated short residence time in the dissolved phase (Romero-Freire et al., 2019; Yuan et al., 2021),

elevated Ga mass fractions might be found within close vicinity of OWFs within the sediment. Nevertheless, current data does not indicate an increasing trend of Ga mass fractions within the period of 2020–2022 or other anthropogenic inputs of Ga into North Sea sediments (Ebeling et al., 2023d).

Similar to Ga no In concentrations of North Sea water have been published up to now. Within this study dissolved In concentrations are within the sub ng L^{-1} range (0.011 ng $L^{-1} \pm 0.001$ ng L^{-1} and 0.27 ng $L^{-1} \pm 0.15$ ng L^{-1}). Alibo et al. (1999) published dissolved In concentration in North Atlantic depth profiles ranging between 0.067 ng L^{-1} and 0.19 ng L^{-1} Whereas the Mediterranean is reported to feature significantly higher In concentrations of around 0.427 ng $L^{-1} \pm 0.067$ ng L^{-1} (Alibo et al., 1999). Due to its high abundance in Al anodes (Reese et al., 2020), as well as extremely low natural background concentrations (abundance of In in the upper continental crust 56 ng g^{-1} (Rudnick and Gao, 2003)) and the lack of other anthropogenic sources offshore, In is the most promising tracer metal for a source assignment related to the dissolution of galvanic anodes. A significant enrichment of In caused by emissions of galvanic anodes will most likely be first observed in the water phase. The elevated In concentrations observed in Area N-4 (2020–2022), Area N-3 (2021) and Area N-6 (2021) may be attributed to accumulations/material emissions that can potentially be caused by the corrosion protection systems. However, also an input of In through the rivers draining into the North Sea could be a source for elevated In concentrations. Therefore, in the following section, the spatial distribution of In is compared to the Gd anomaly as a tracer for riverine input.

4.2. Source assignment for variations of metal concentrations

To further investigate the possible origin of the elevated In concentrations, they are compared to Gd anomalies and drift trajectories of the sampled water masses for all campaigns in chronological order.

In 2016 (see Fig. 5 (top)) mainly Area N-4 was sampled. The Gd anomaly showed medium to high values within Area N-4 and the drift trajectory indicates that the sampled water mass originates from the coastal area. In concentrations ranged between 0.0521 ng $L^{-1} \pm 0.0013$ ng L^{-1} and 0.1482 ng $L^{-1} \pm 0.067$ ng L^{-1}. This data indicates anthropogenic (coastal) impact, which is likely riverine input from the Elbe, whose effect on this area was already shown in previous studies (Böhnecke, 1922; Ebeling et al., 2023d).

In 2018 the Gd anomaly was elevated in Area N-3 (average 2.2) compared to Area N-2 and Area N-4, which showed an average Gd anomaly of 1.7 and 1.8, respectively. The In concentrations in the samples of this year were all below LOQ (0.051 ng L^{-1}) or even LOD (0.0069 ng L^{-1}). Overall, sampling sites with a higher Gd anomaly (Area N-3, northern part of Area N-4) tend to show In concentrations above the
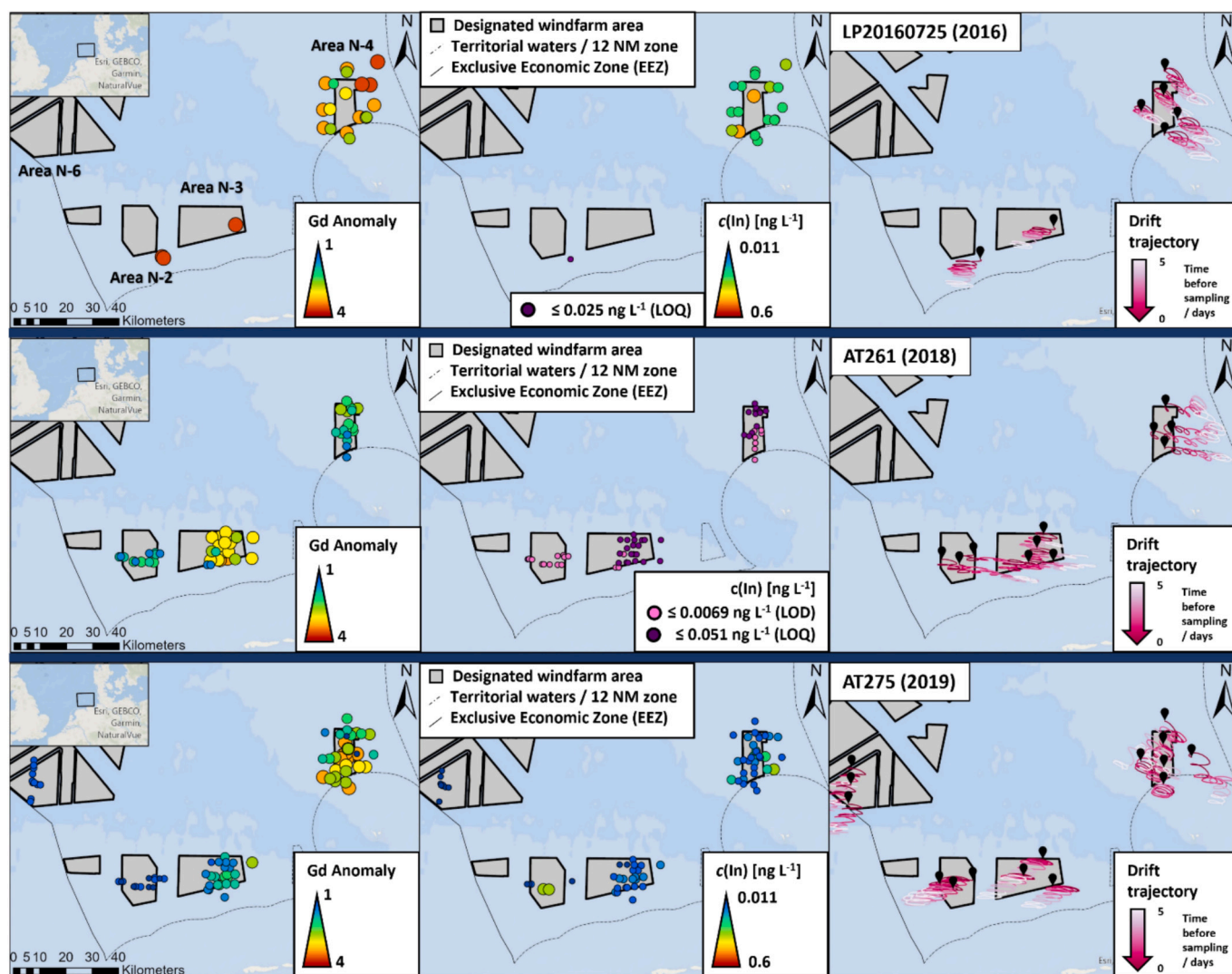
Fig. 5. Spatial distribution of (from left to right) Gd anomaly, In concentration and back trajectory of water masses for selected sample sights in North Sea waters in and around OWFs of the German Bight in 2016 (top), 2018 (middle) and 2019 (bottom). The investigated areas are grouped according to the official designation of the site development plan for the German North Sea and Baltic Sea by the BSH (BSH, 2023b).

LOD while sampling sites with a lower Gd anomaly (Area N-2, southern part of Area N-4) tend to show In concentrations below LOD (see Fig. 5 (middle)). This might indicate a riverine influence of the In concentrations. The drift trajectory showed water mass movement from the east, which could explain why Area N-3 is more anthropogenically impacted than Area N-2, as water masses from the coastal area need to move through Area N-3 to reach Area N-2. Moreover, the pattern of the Gd anomaly in Area N-4 is also comparable for Zn and Al concentrations, with higher values in the north compared to the south (see ESM Figs. A5 and A7). The drift trajectories support the assumption that these increases in concentration and anomaly are due to coastal inputs.

The stations sampled in 2019 in Fig. 5 (bottom) show no clear trend. Area N-2, N-3 and N-6 featured a medium to low Gd anomaly with most medium values (1.24–1.98) found in Area N-3. In concentrations in these areas are low with two stations in Area N-2 showing slightly higher concentrations. The higher Gd anomaly in Area N-3 might be due to its proximity to the coast compared to Area N-2 and N-6. Area N-4 showed an elevated Gd anomaly with higher anomalies found in the southern half compared to the stations located further north. In concentrations are mainly low and no visible correlation to the Gd anomaly is evident. The drift trajectory shows complex water mass mixing. Water masses circled mainly within the wind farm area. The combination of the data

indicates some kind of anthropogenic influence within this area in 2019 showing no visible accumulation of In. However, Cd and Zn concentrations in Area N-4 are elevated compared to all other sampled areas (ESM Figs. A1 and A7). The Al and Ga concentrations in Area N-4 show higher concentrations in the north than in the south. While the increasing gradient in Al and Ga concentrations together with an inverted trend in the Gd anomaly and drift trajectories indicating water masses travelling through the wind farms suggests that the sampled water is impacted by metal inputs from OWFs, Cd and Zn concentrations do not support this hypothesis. However, the elevated Cd and Zn concentrations might originate from multiple sources and superimpose the pure OWF signal.

As shown in Fig. 3C elevated In concentrations were measured mainly around Area N-4. The spatial distribution indicates a North-South gradient within Area N-4 in 2020 with the highest In concentrations found in the northern half (see Fig. 6 (top)). An opposing trend can be seen for the Gd anomaly, showing lower values in the northern part. The drift trajectory shows limited water mass movement five days prior to sampling. The sampling station at the southern end of Area N-4 shows a slightly higher water mass movement prior to sampling with a trajectory coming eastwards from the coast. All information combined, the water sampled in the southern half of Area N-4 shows slightly elevated
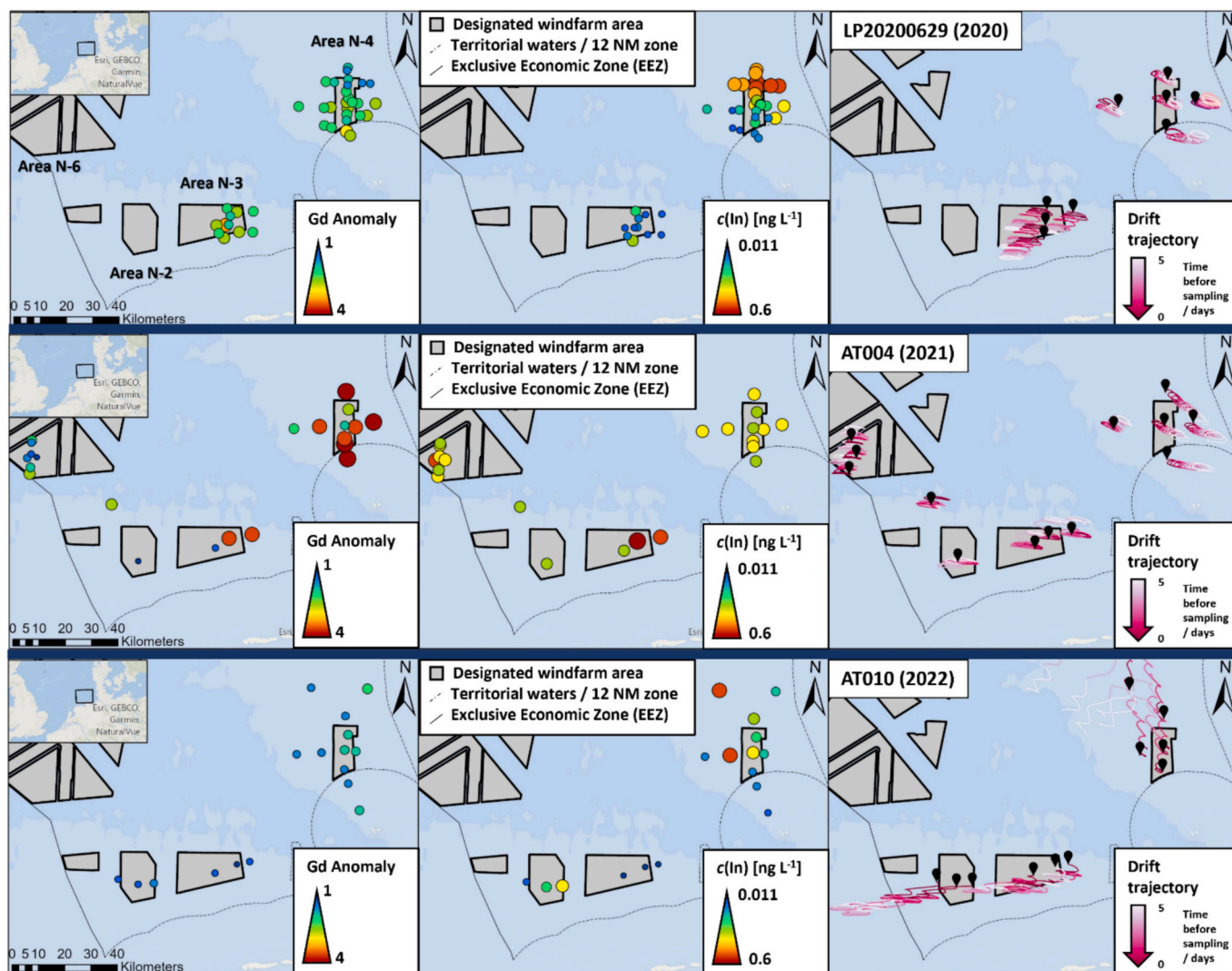
Fig. 6. Spatial distribution of (from left to right) Gd anomaly, In concentration and back trajectory of water masses for selected sample sights in North Sea waters in and around OWFs of the German Bight in 2020 (top), 2021 (middle) and 2022 (bottom). The investigated areas are grouped according to the official designation of the site development plan for the German North Sea and Baltic Sea by the BSH (BSH, 2023b).

Gd anomaly that was transported from coastal and/or riverine waters (most likely from the Elbe river (Böhnecke, 1922; Ebeling et al., 2023d)) to the OWF while the sampled waterbody in the northern half of Area N-4 circulated within a tight radius in the OWF accumulating In from galvanic anodes.

In 2021 elevated In concentrations were observed in Area N-3, and Area N-6 and slightly elevated In concentrations in Area N-4 (see Fig. 3C). As shown in Fig. 6 (middle) Area N-3 and Area N-4 feature elevated Gd anomalies indicating an influence by coastal and riverine inputs. This assumption is supported by the drift trajectories that show that the water masses in both areas originate predominantly from outside the sampling area. For Area N-4 the water masses originate again from the south-east (coastal area) indicating riverine input from the Elbe. For Area N-3 the drift trajectory indicates that the water masses originated from north-east of the OWF which is opposite to the flow direction of the Elbe plume. In Area N-6, which is furthest away from the coast, no elevated Gd anomaly was evident, indicating a low coastal impact, while elevated In concentrations were found. Combined with the drift trajectory, this indicates that water masses circled within the OWF area five days before sampling. Therefore, the In concentrations probably originate from a source within the OWF.

Fig. 6 (bottom) shows a data comparison for the campaign in 2022. Elevated In concentrations were found in Area N-4 (see Fig. 3C).

Elevated In concentrations (red circles, Fig. 6 (bottom)) were found at two sampling stations outside the OWF. Overall, the Gd anomaly was found to be low for all sampling locations in 2022. The drift trajectory indicates a strong water mass movement within five days before sampling, leading to increased water mass mixing. This hinders the accurate assessment of possible sources.

Overall, a total of two individual events (Area N-4 in 2020 and Area N-6 in 2021) were identified in six years in which elevated dissolved In concentrations are likely due to the corrosion protection of OWFs. Both cases featured minor to no water mass mixing with five days prior to sampling and a low Gd anomaly indicating minor anthropogenic influence, e.g. through rivers.

5. Conclusions

Currently available studies on metal emissions related to galvanic anodes from OWFs emphasize the need for further investigations to assign possible emissions of OWFs with higher confidence. As the traditionally monitored metals Cd, Pb and Zn have a variety of anthropogenic sources, high abundances, combined with complex and dynamic ocean currents, source tracing based on these three metals is very challenging. This study does not indicate measurable inputs of these metals clearly attributed to OWFs. Cd and Pb concentration ranges were

mainly within known concentration ranges of regular monitoring data with locally elevated concentrations in 2019, 2021 and 2022. Zn showed a higher variability, but all measured concentrations were within the range of regular monitoring data. Consideration of these three elements alone is not sufficient for a clear allocation of emissions caused by OWFs.

Although Al is the main component of Al-based galvanic anodes, dissolved Al did not show elevated concentrations relatable to OWFs. Furthermore, all measured Al concentrations in this study were below known concentrations and showed no clear trend.

Especially In has been proven to be a powerful tracer metal for the monitoring of galvanic anode emissions in seawater. Elevated In concentrations were found in this study, while Ga concentrations were within the comparison data. Indeed, reliable reference values for both metals are scarce and no background concentrations of the North Sea are available. This study provides the first Ga and In concentrations as a basis for future investigations. Results of this study also suggest that source attribution solely based on concentration data is limited. The combination of In concentrations, Gd anomaly and drift trajectory of water masses showed a high potential for an in-depth source assignment. The release of In caused by the dissolution of galvanic anodes seems to be associated to OWFs corrosion protection for at least one area in two years (Area-N4, 2020 and Area-N6 in 2021), covering two of the elevated In concentration ranges found in this study (up to 0.269 ng L^{-1} $\pm$ 0.028 ng L^{-1} and up to 0.24 ng L^{-1} $\pm$ 0.06 ng L^{-1}, respectively). Both cases were associated with low water mass movement for at least several days before sampling. This finding also supports the hypothesis of a rapid dilution of OWFs related emissions under more turbulent conditions. Future campaigns should therefore aim to match sampling to time frames with low water mass movement.

The presented combination of In concentrations with Gd anomaly and back trajectory of water masses is a very promising approach for source tracing. It can provide information on the origin of locally increased metal concentrations especially for OWFs in close proximity to the coast. Even though, other natural or anthropogenic sources for the observed elevated In concentrations cannot be ruled out completely, it is evident that galvanic anodes are per se a continuous source of metal emissions and represent a new source in the marine environment from OWFs. Yet, operation and expansion of offshore wind energy will continue. Therefore, further investigations should contribute to better assess possible medium- to long-term effects of such chemical emissions on the marine environment. In this context, future OWF projects should also consider alternative corrosion protections techniques during their planning to reduce potential chemical emissions to a minimum.

CRediT authorship contribution statement

Anna Ebeling: Writing – original draft, Visualization, Validation, Investigation, Formal analysis, Data curation, Conceptualization. **Dominik Wippermann:** Writing – original draft, Visualization, Investigation, Formal analysis, Data curation, Conceptualization. **Tristan Zimmermann:** Writing – review & editing, Writing – original draft, Validation, Methodology, Investigation, Formal analysis. **Ole Klein:** Writing – original draft, Visualization, Validation, Methodology, Formal analysis, Data curation. **Torben Kirchgeorg:** Writing – review & editing, Resources, Project administration, Conceptualization. **Ingo Weinberg:** Writing – review & editing, Resources, Project administration, Conceptualization. **Anna Plass:** Writing – review & editing, Project administration. **Simone Hasenbein:** Writing – review & editing, Resources, Conceptualization. **Daniel Pröfrock:** Writing – review & editing, Writing – original draft, Supervision, Resources, Project administration, Methodology, Investigation, Funding acquisition, Conceptualization.

Declaration of competing interest

Acknowledgments

Appendix A. Supplementary data

Supplementary data to this article can be found online at https://doi.org/10.1016/j.marpolbul.2025.117810.

Data availability

Data will be made available on request.

References

Alibo, D.S., Nozaki, Y., Jeandel, C., 1999. Indium and yttrium in North Atlantic and Mediterranean waters: comparison to the Pacific data. Geochim. Cosmochim. Acta 63, 1991–1999. https://doi.org/10.1016/s0016-7037(99)00080-0.

ANZECC, ARMCANZ, 2000. Australian and New Zealand guidlines for fresh and marine water quality, in: Australian and New Zealand environment and conservation council & agriculture and resource Management Council of Australia and new Zealand (Ed.). https://www.waterquality.gov.au/sites/default/files/documents/anzecc-armcanz-2000-guidelines-vol1.pdf.

ArcGIS, 2023. Ocean base, sources: Esri, GEBCO, NOAA, national geographic, DeLorme, HERE, Geonames.org, and other contributors. https://services.arcgisonline.com/arcgis/rest/services/Ocean/World_Ocean_Base/MapServer. (Accessed 7 April 2023).

Bau, M., Dulski, P., 1996. Anthropogenic origin of positive gadolinium anomalies in river waters. Earth Planet. Sci. Lett. 143, 245–255. https://doi.org/10.1016/0012-821X(96)00127-6.

Bird, P., Comber, S.D.W., Gardner, M.J., Ravenscroft, J.E., 1996. Zinc inputs to coastal waters from sacrificial anodes. Sci. Total Environ. 181, 257–264. https://doi.org/10.1016/0048-9697(95)05025-6.

Böhnecke, G., 1922. Salzgehalt und Strömungen der Nordsee. Zeitschrift der Gesellschaft für Erdkunde zu Berlin 300–302.

Bruland, K.W., 1980. Oceanographic distributions of cadmium, zinc, nickel, and copper in the North Pacific. Earth Planet. Sci. Lett. 47, 176–198. https://doi.org/10.1016/0012-821x(80)90035-7.

BSH, 2016. Nordseezustand 2008–2011. Hamburg and Rostock. https://www.bsh.de/DE/PUBLIKATIONEN/_Anlagen/Downloads/Meer_und_Umwelt/Berichte-des-BSH/Berichte-des-BSH_54.html.

BSH, 2023a. Flächenentwicklungsplan 2023 - WMS. available online at https://www.geoseaportal.de/wss/service/Site_Development_Plan_2023/guest?SERVICE=WMS&REQUEST=GetCapabilities&VERSION=1.3.0. (Accessed 7 April 2023).

BSH, 2023b. Flächenentwicklungsplan 2023 für die deutsche Nordsee und Ostsee. Hamburg and Rostock. https://www.bsh.de/DE/THEMEN/Offshore/Meeresfachplanung/Flaechenentwicklungsplan/_Anlagen/Downloads/FEP_2023_1/Flaechentwicklungsplan_2023.pdf?__blob=publicationFile&v=1.

Callies, U., 2021. Sensitive dependence of trajectories on tracer seeding positions – coherent structures in German Bight backward drift simulations. Ocean Sci. 17, 527–541. https://doi.org/10.5194/os-17-527-2021.

Callies, U., Plüß, A., Kappenberg, J., Kapitza, H., 2011. Particle tracking in the vicinity of Helgoland, North Sea: a model comparison. Ocean Dyn. 61, 2121–2139. https://doi.org/10.1007/s10236-011-0474-8.

Callies, U., Groll, N., Horstmann, J., Kapitza, H., Klein, H., Maßmann, S., Schwichtenberg, F., 2017. Surface drifters in the German Bight: model validation considering windage and Stokes drift. Ocean Sci. 13, 799–827. https://doi.org/10.5194/os-13-799-2017.

Christiansen, N., Daewel, U., Schrum, C., 2022. Tidal mitigation of offshore wind wake effects in coastal seas. Front. Mar. Sci. 9, 1–15. https://doi.org/10.3389/fmars.2022.1006647.

de Laeter, J.R., Böhlke, J.K., De Bièvre, P., Hidaka, H., Peiser, H.S., Rosman, K.J.R., Taylor, P.D.P., 2003. Atomic weights of the elements. Review 2000 (IUPAC technical report). Pure Appl. Chem. 75. https://doi.org/10.1351/pac200375060683.

Degraer, S., Brabant, R., Rumes, B., Vigin . (eds.), L., Degraer, S., et al. (Eds.), 2019. Environmental Impacts of Offshore Wind Farms in the Belgian Part of the North Sea: Marking a Decade of Monitoring, Research and Innovation. Royal Belgian Institute of Natural Sciences, O.N.E., Marine Ecology and Management, Brussels, p. 134. https://tethys.pnnl.gov/publications/environmental-impacts-offshore-wind-farms-belgian-part-north-sea-marking-decade.

Degraer, S., Brabant, R., Rumes, B., Vigin, L., 2021. Environmental impacts of offshore wind farms in the Belgian part of the North Sea. In: Attraction, Avoidance And Habitat Use at Various Spatial Scales.

Deutsche WindGuard GmbH, 2024. Status des Offshore-Windenergieausbaus in Deutschland - Erstes Halbjahr 2024. Varel. https://www.windguard.de/Statistik-1-Halbjahr-2024.html?file=files/cto_layout/img/unternehmen/windenergiestatistik/2024/Halbjahr/Status%20des%20Offshore-Windenergieausbaus_Halbjahr%202024.pdf.

DIN e.V (Ed.), 2008. DIN 32645:2008-11: Chemical Analysis - Decision Limit, Detection Limit and Determination Limit Under Repeatability Conditions - Terms, Methods, Evaluation, pp. 1–28.

Ebeling, A., Zimmermann, T., Klein, O., Irrgeher, J., Pröfrock, D., 2022. Analysis of seventeen certified water reference materials for trace and technology-critical elements. Geostand. Geoanal. Res. https://doi.org/10.1111/ggr.12422.

Ebeling, A., Klein, O., Voigt, N., Pröfrock, D., 2023a. Trace metal distribution for water samples of Atair cruise AT275 [dataset]. In: PANGAEA (Ed.).

Ebeling, A., Rust, B., Klein, O., El Gareb, F.R., Erbslöh, H.-B., Pieper, A., Pröfrock, D., 2023b. Trace metal distribution for water samples of Ludwig Prandtl cruise LP20200629 [dataset]. In: PANGAEA (Ed.).

Ebeling, A., Rust, B., Zimmermann, T., Pröfrock, D., 2023c. Trace metal distribution for water samples of ATAIR cruise AT261 [dataset]. In: PANGAEA (Ed.).

Ebeling, A., Wippermann, D., Zimmermann, T., Klein, O., Kirchgeorg, T., Weinberg, I., Hasenbein, S., Plass, A., Pröfrock, D., 2023d. Investigation of potential metal emissions from galvanic anodes in offshore wind farms into North Sea sediments. Mar. Pollut. Bull. 194, 115396. https://doi.org/10.1016/j.marpolbul.2023.115396.

EU, 2008. DIRECTIVE 2008/105/EC OF THE EUROPEAN PARLIAMENT AND OF THE COUNCIL, Official Journal of the European Union, pp. L 348/384 - L 348/397.

Eurachem/Citac, 2012. EURACHEM/CITAC guide: Quantifying Uncertainty in Analytical Measurements, 3 ed.

Gabelle, C., Baraud, F., Biree, L., Gouali, S., Hamdoun, H., Rousseau, C., van Veen, E., Leleyter, L., 2012. The impact of aluminium sacrificial anodes on the marine environment: a case study. Appl. Geochem. 27, 2088–2095. https://doi.org/10.1016/j.apgeochem.2012.07.001.

Golding, L.A., Angel, B.M., Batley, G.E., Apte, S.C., Krassoi, R., Doyle, C.J., 2015. Derivation of a water quality guideline for aluminium in marine waters. Environ. Toxicol. Chem. 34, 141–151. https://doi.org/10.1002/etc.2771.

GWEC, 2024. Global wind report 2024. Brussels. https://gwec.net/global-wind-report-2024/.

Hatje, V., Bruland, K.W., Flegal, A.R., 2016. Increases in anthropogenic gadolinium anomalies and rare earth element concentrations in San Francisco Bay over a 20 year record. Environ. Sci. Technol. 50, 4159–4168. https://doi.org/10.1021/acs.est.5b04322.

Kirchgeorg, T., Weinberg, I., Hörnig, M., Baier, R., Schmid, M.J., Brockmeyer, B., 2018. Emissions from corrosion protection systems of offshore wind farms: evaluation of the potential impact on the marine environment. Mar. Pollut. Bull. 136, 257–268. https://doi.org/10.1016/j.marpolbul.2018.08.058.

Klein, O., Zimmermann, T., Petrauskas, C., Ebeling, A., Pieper, A., Irrgeher, J., Pröfrock, D., 2022. Trace metal distribution for water samples of Ludwig Prandtl cruise LP20160725 [dataset]. In: PANGAEA (Ed.).

Komárek, M., Ettler, V., Chrastný, V., Mihaljevič, M., 2008. Lead isotopes in environmental sciences: a review. Environ. Int. 34, 562–577. https://doi.org/10.1016/j.envint.2007.10.005.

Kremling, K., Andreae, M.O., Brgmann, L., van den Berg, C.M.G., Prange, A., Schirmacher, M., Koroleff, E., Kremling, K., Kus, J., 1999. In: Grasshoff, K., et al. (Eds.), Determination of Trace Elements, 3 ed. Wiley-VCH Verlag GmbH, Weinheim, Germany, pp. 253–364. https://doi.org/10.1002/9783527613984.ch12.

Kulaksız, S., Bau, M., 2007. Contrasting behaviour of anthropogenic gadolinium and natural rare earth elements in estuaries and the gadolinium input into the North Sea. Earth Planet. Sci. Lett. 260, 361–371. https://doi.org/10.1016/j.epsl.2007.06.016.

McLennan, S.M., 1989. Rare earth elements in sedimentary rocks influence of provenance and sedimentary processes. Rev. Mineral. Geochem. 21, 169–200.

Nozaki, Y., Thomson, J., Turekian, K.K., 1976. The distribution of 210Pb and 210Po in the surface waters of the Pacific Ocean. Earth Planet. Sci. Lett. 32, 304–312. https://doi.org/10.1016/0012-821x(76)90070-4.

Orians, K.J., Bruland, K.W., 1986. The biogeochemistry of aluminum in the Pacific Ocean. Earth Planet. Sci. Lett. 78, 397–410. https://doi.org/10.1016/0012-821x(86)90006-3.

OSPAR, 2005. Agreement on Background Concentrations for Contaminants in Seawater, Biota and Sediment. OSPAR Agreement 2005-6, pp. 1–4.

OSPAR, 2009a. Background document on CEMP assessment criteria for QSR 2010. Monit. Assess. Series, 461/2009.

OSPAR, 2009b. Losses of contaminants from ships' coatings and anodes. https://qsr2010.ospar.org/media/assessments/p00462_Leaching_report.pdf.

Prange, A., Bössow, E., Erbslöh, B., Jablonski, R., Jantzen, E., Kause, P., Krüger, F., Lenart, H., Leonhard, P., Meyercordt, J., Niedergesäß, R., Pepelnik, R., von Tümpling, W., 2001. Grafische Darstellung der Längsprofile - Filtarte, Schwebnstoffe, Sedimente, Neue, erwei ed. GKSS-Forschungszentrum Geesthacht GmbH, Geesthacht.

Przibilla, A., Iwainski, S., Zimmermann, T., Pröfrock, D., 2023. Impact of storage temperature and filtration method on dissolved trace metal concentrations in coastal water samples. Water Environ. Res. 95, e10922. https://doi.org/10.1002/wer.10922.

Reese, A., Voigt, N., Zimmermann, T., Irrgeher, J., Pröfrock, D., 2020. Characterization of alloying components in galvanic anodes as potential environmental tracers for heavy metal emissions from offshore wind structures. Chemosphere 257, 127182. https://doi.org/10.1016/j.chemosphere.2020.127182.

Romero-Freire, A., Santos-Echeandía, J., Neira, P., Cobelo-García, A., 2019. Less-studied technology-critical elements (Nb, Ta, Ga, In, Ge, Te) in the marine environment: review on their concentrations in water and organisms. Front. Mar. Sci. 6. https://doi.org/10.3389/fmars.2019.00532.

Rudnick, R.L., Gao, S., 2003. Composition of the continental crust. Elsevier 1–64. https://doi.org/10.1016/B0-08-043751-6/03016-4.

Schulz-Stellenfleth, J., Blauw, A., Laakso, L., Mourre, B., She, J., Wehde, H., 2023. Fit-for-purpose information for offshore wind farming applications—part-II: gap analysis and recommendations. J. Mar. Sci. Eng. 11, 1817. https://doi.org/10.3390/jmse11091817.

Siems, A., Zimmermann, T., Sanders, T., Pröfrock, D., 2024. Dissolved trace elements and nutrients in the North Sea-a current baseline. Environ. Monit. Assess. 196, 539. https://doi.org/10.1007/s10661-024-12675-2.

UBA, 2024. MUDAB Meeresumweltdatenbank. available online at https://geoportal.bafg.de/MUDABAnwendung/. accessed on 2024.

VGB/BAW, 2018. VGB-S-021-04-2018-07-EN, VGB/BAW Standard Corrosion Protection for Offshore Wind Structures Part 4: Cathodic Protection (CP).

Wang, T., Ru, X., Deng, B., Zhang, C., Wang, X., Yang, B., Zhang, L., 2023. Evidence that offshore wind farms might affect marine sediment quality and microbial communities. Sci. Total Environ. 856, 158782. https://doi.org/10.1016/j.scitotenv.2022.158782.

Wippermann, D., Faust, S., Zimmermann, T., Pröfrock, D., 2025a. Trace metal distribution for water samples of the cruise AT010 [dataset]. In: PANGAEA (Ed.).

Wippermann, D., Pieper, A., Zimmermann, T., Klein, O., Pröfrock, D., 2025b. Trace metal distribution for water samples of the cruise AT004 [dataset]. In: PANGAEA (Ed.).

Wright, A.J., Araújo-Wang, C., Wang, J.Y., Ross, P.S., Tougaard, J., Winkler, R., Márquez, M.C., Robertson, F.C., Williams, K.F., Reeves, R.R., 2020. How 'blue' is 'green' energy? Trends Ecol. Evol. 35, 235–244. https://doi.org/10.1016/j.tree.2019.11.002.

Wuttig, K., Townsend, A.T., van der Merwe, P., Gault-Ringold, M., Holmes, T., Schallenberg, C., Latour, P., Tonnard, M., Rijkenberg, M.J.A., Lannuzel, D., Bowie, A. R., 2019. Critical evaluation of a seaFAST system for the analysis of trace metals in marine samples. Talanta 197, 653–668. https://doi.org/10.1016/j.talanta.2019.01.047.

Yuan, W., Chen, J., Teng, H., Chetelat, B., Cai, H., Liu, J., Wang, Z., Bouchez, J., Moynier, F., Gaillardet, J., Schott, J., Liu, C., 2021. A review on the elemental and isotopic geochemistry of gallium. Global Biogeochem. Cycles 35. https://doi.org/10.1029/2021gb007033.

Zimmermann, T., Mohamed, A.F., Reese, A., Wieser, M.E., Kleeberg, U., Pröfrock, D., Irrgeher, J., 2020. Zinc isotopic variation of water and surface sediments from the German Elbe River. Sci. Total Environ. 707, 135219. https://doi.org/10.1016/j.scitotenv.2019.135219.